A&A 559, A39 (2013)
DOI: 10.1051/0004-6361/201220816

Astronomy & Astrophysics

Stellar granulation as seen in disk-integrated intensity

I. Simplified theoretical modeling⋆

R. Samadi[1], K. Belkacem[1], and H.-G. Ludwig[2,3]

[1] LESIA, Observatoire de Paris, CNRS UMR 8109, UPMC, Université Denis Diderot, 5 place Jules Janssen, 92195 Meudon Cedex, France
e-mail: reza.samadi@obspm.fr
[2] Zentrum für Astronomie der Universität Heidelberg, Landessternwarte, Knigstuhl 12, 69117 Heidelberg, Germany
[3] GEPI, Observatoire de Paris, CNRS UMR 8111, Université Denis Diderot, 5 place Jules Janssen, 92195 Meudon Cedex, France

Received 29 November 2012 / Accepted 4 September 2013

ABSTRACT

Context. Solar granulation has been known for a long time to be a surface manifestation of convection. The space-borne missions CoRoT and *Kepler* enable us to observe the signature of this phenomena in disk-integrated intensity on a large number of stars.
Aims. The space-based photometric measurements show that the global brightness fluctuations and the lifetime associated with granulation obeys characteristic scaling relations. We thus aimed at providing simple theoretical modeling to reproduce these scaling relations, and subsequently at inferring the physical properties of granulation across the Hertzsprung-Russell diagram.
Methods. We developed a simple 1D theoretical model. The input parameters were extracted from 3D hydrodynamical models of the surface layers of stars, and the free parameters involved in the model were calibrated with solar observations. Two different prescriptions for representing the Fourier transform of the time-correlation of the eddy velocity were compared: a Lorentzian and an exponential form. Finally, we compared our theoretical prediction with 3D radiative hydrodynamical (RHD) numerical modeling of stellar granulation (hereafter ab initio approach).
Results. Provided that the free parameters are appropriately adjusted, our theoretical model reproduces the observed solar granulation spectrum quite satisfactorily; the best agreement is obtained for an exponential form. Furthermore, our model results in granulation spectra that agree well with the ab initio approach using two 3D RHD models that are representative of the surface layers of an F-dwarf and a red-giant star.
Conclusions. We have developed a theoretical model that satisfactory reproduces the solar granulation spectrum and gives results consistent with the ab initio approach. The model is used in a companion paper as theoretical framework for interpretating the observed scaling relations.

Key words. convection – turbulence – Sun: granulation

1. Introduction

The solar surface reveals irregular cellular patterns commonly called granules. These structures were first discovered and discussed during the 19th century (see an historical review in Bray & Loughhead 1967). Their origin was first attributed by Unsöld (1930) to convective currents occuring beneath the visible photospheric layers, while their turbulent nature was first highlighted by Siedentopf (1933). Several decades later, with the advances in numerical hydrodynamical simulations, the properties of solar granulation are well explained (e.g. Muller 1999, and references therein).

Stars with effective temperatures lower than about 7000 K have an appreciable upper convective envelope and are thus expected to show – as in the Sun – granules on their surface. Because the granules evolve with time, their evolution produces small brightness fluctuations that can now be accurately monitored and measured with space-based high-precision photometry measurements performed with the MOST, CoRoT, and *Kepler* missions (Matthews et al. 2004; Michel et al. 2008; Kallinger & Matthews 2010; Mathur et al. 2011; Chaplin et al. 2011b). These observations reveal that the characteristic time $\tau_{\rm eff}$ of the granules and the total brightness fluctuations σ associated with them scales as a function of the frequency $\nu_{\rm max}$ at which the solar-like oscillations peak (e.g., Huber et al. 2009; Kallinger & Matthews 2010; Chaplin et al. 2011b; Mathur et al. 2011; Kjeldsen & Bedding 2011). In turn, $\nu_{\rm max}$ is shown to scale with the cut-off frequency $\nu_{\rm c}$ of the atmosphere, therefore mainly the pressure scale-height near the photosphere (Brown et al. 1991; Kjeldsen & Bedding 1995; Stello et al. 2009; Huber et al. 2009; Mosser et al. 2010; Belkacem et al. 2011). The observed relation between the properties of the stellar granulation and $\nu_{\rm c}$ were explained on the basis of some simplified physical considerations (Huber et al. 2009; Kjeldsen & Bedding 2011; Mathur et al. 2011). A detailed theoretical study of the observed scaling relations is, however, lacking.

A possible theoretical approach is the one proposed by Ludwig (2006). This ab initio approach consists of modeling the stellar granulation as seen in disk-integrated intensity from the intensity emerging *directly* from given 3D radiative hydrodynamical (RHD) models. This numerical approach was applied by several authors (Svensson & Ludwig 2005; Ludwig et al. 2009; Mathur et al. 2011). It is very time-consuming and hence does not easily allow envisaging a large set of calculations with different surface metal abundance, for example. Furthermore,

⋆ Appendices are available in electronic form at http://www.aanda.org

interpreting the results is not trivial, and the systematic differences obtained by Mathur et al. (2011) between observed and modeled spectra of red giants are not well understood. On the other hand, a theoretical model based on a more simplified physical approach offers the advantage of separately testing several properties of turbulent convection. In addition, it allows one to compute the granulation spectrum for a variety of stars on a large scale. Furthermore, it is possible to derive scaling relations from such a simplied theoretical model that could provide additional theoretical support for the observed scaling relations and extend the current theoretical scaling relations. We here present such a simple theoretical model of the stellar granulation as seen in disk-integrated intensity. In the companion paper (Samadi et al. 2013, hereafter Paper II), we derive theoretical scaling relations for σ and $\tau_{\rm eff}$ from this model. Comparisons with a large sample of observed stars as well as with previously published scaling relations are reported in Paper II.

This Paper I is organized as follows: in Sect. 2, we outline our theoretical model for the stellar granulation spectrum in disk-integrated intensity and the different prescriptions adopted for modeling the properties of turbulent granules. The free parameters introduced in the theoretical model are next calibrated in Sect. 3 such that our theoretical calculations match at best the solar observations. In Sect. 4, we compare our calculations with those obtained with the ab initio approach of Ludwig (2006) using two 3D RHD models of the surface layers of an F-dwarf star and a red giant star. Finally, Sect. 5 is devoted to the conclusion.

2. Modeling of the power density spectrum

We here outline our theoretical model for the power spectrum associated with the relative variations of the bolometric flux emerging from the star in the direction of an observer, who would measure it continuously during a given duration (typically much longer than the timescale of the granulation). The detailed derivation of the model is presented in Appendix A, while the underlying approximations and assumptions are discussed in Appendix B.

$F(t)$ is the bolometric flux toward the observer at the instant t, and we define $\Delta F(t) = F(t) - \langle F\rangle_t$ as the instantaneous variation of the flux with respect to its time average, $\langle F\rangle_t$. From now on $\langle\rangle\, t$ stands for a time average. The power density spectrum (PDS) associated with the relative variation of the flux $(\Delta F(t)/\langle F\rangle_t)$ is hence defined by

$$\mathcal{F}(\nu) = \frac{1}{T_0}\frac{\left|\widehat{\Delta F}\right|^2}{\langle F\rangle_t^2}, \tag{1}$$

where T_0 is the duration of the observation, and ν a given frequency. The operator $\widehat{(\,.\,)}$ is

$$\widehat{f}(\nu) = \int_{-T_0/2}^{T_0/2} \mathrm{d}t\, f(t)\, \mathrm{e}^{\mathrm{i}\,2\pi\nu t}. \tag{2}$$

We point out that with CoRoT or *Kepler* observations T_0 is typically much longer than the granule lifetime such that the operator $\widehat{(\,.\,)}$ tends to the classical Fourier transform.

We consider a *gray atmosphere*. This is a necessary condition to obtain an analytical formulation for the granulation spectrum. We adopt a spherical coordinate system (r, θ, ϕ) with the z-axis pointing toward the observer. Accordingly, the bolometric flux received from the star at the instant t is given by

$$F(t) = R_{\rm s}^2 \int_{\phi=0}^{2\pi} \mathrm{d}\phi \int_{\mu=0}^{1} \mathrm{d}\mu\, \mu\, I(t, \tau = 0, \mu, \phi), \tag{3}$$

where $\mu = \cos(\theta)$, $I(t, \tau, \mu, \phi)$ is the specific intensity in the direction (μ, ϕ), $R_{\rm s}$ the radius of the star, and $\tau(r)$ the mean optical depth

$$\tau(r) = \int_{r'=r}^{+\infty} \mathrm{d}r'\, \kappa(r')\, \overline{\rho}(r'), \tag{4}$$

where κ is the mean opacity, $\overline{\rho}$ is the mean density (i.e., averaged in time and over a sphere of radius r) and the specific intensity $I(\tau, \mu, \phi)$ is related to the source function according to (e.g., Gray 1992, p. 114)

$$I(\tau, \mu, \phi) = \int_{\tau}^{+\infty} \mathrm{d}\tau'\, \frac{\mathrm{e}^{-\tau'(r)/\mu}}{\mu}\, S\,(t, \tau'(r), \mu, \phi), \tag{5}$$

where S is the source function.

To proceed, we assume the local thermodynamic equilibrium (LTE) so that $S = B$, where B is the Planck function at the instant t and the position $(\tau(r), \mu, \phi)$. Note that LTE is fully justified because the region where the granules are seen most often extends to the small region around the optical depth $\tau \sim 1$ (i.e., near the photosphere). Accordingly, and using Eqs. (3) and (5), $\Delta F(t)$ is rewritten such as

$$\Delta F(t) = R_{\rm s}^2 \int_{\phi=0}^{2\pi} \mathrm{d}\phi \int_{\mu=0}^{1} \mathrm{d}\mu \int_{0}^{+\infty} \mathrm{d}\tau\, \mathrm{e}^{-\tau(r)/\mu}\, \Delta B, \tag{6}$$

where we have defined $\Delta B \equiv B - \langle B\rangle_t$.

We neglect length-scales longer than the granulation length-scales. In that case ΔB represents the instantaneous difference between the brightness of the granules situated at position $(\tau(r), \mu, \phi)$ and the brightness of the material in the steady state ($\langle B\rangle_t$). Finally, we assume that $\kappa\rho$ varies at a length-scale longer than the characteristic size of the granule. From this set of assumptions, and after some calculations, Eq. (1) can be written (see details in Appendix A)

$$\mathcal{F}(\nu) = \int_0^1 \mathrm{d}\mu \int_0^{+\infty} \mathrm{d}\tau\, \mathrm{e}^{-2\tau/\mu} \left(\frac{\langle B\rangle_t}{F_0}\right)^2 \mathcal{F}_\tau(\tau, \nu) \tag{7}$$

with

$$\mathcal{F}_\tau(\tau, \nu) = \frac{(2\pi)^2\,\kappa\rho}{R_{\rm s}^2\,\langle B\rangle_t^2}\, \langle \Delta\widetilde{B_1}\, \Delta B_2\rangle(\nu, \boldsymbol{k} = \boldsymbol{0}, \tau), \tag{8}$$

where the constant F_0 is given by Eq. (A.15), $\langle \Delta\widetilde{B_1}\, \Delta B_2\rangle(\nu, \boldsymbol{k}, \tau)$ is the space and time Fourier transform of $\langle \Delta B_1\, \Delta B_2\rangle$ (see Eq. (A.13)), where k is a wavenumber, ν a frequency, and the subscripts 1 and 2 refer to two different spatial and temporal positions.

To continue we need to derive an expression for the correlation product $\langle \Delta B_1\, \Delta B_2\rangle$. To this end, we recall that $B = \sigma T^4/\pi$, where σ is the Stefan-Boltzmann constant, and introduce ΔT as the difference between the temperature of the granule and that of the surrounding medium. We further more use the quasi-normal approximation (Millionshchikov 1941) and assume that the scalar $\Theta \equiv \Delta T/\langle T\rangle_t$ is isotropic and behaves as a passive scalar. $E_\Theta(k, \nu)$ is then introduced as its associated spectrum (Lesieur 1997, Chap. V-10) and factorized into a spatial spectrum $E_\Theta(k)$ and a frequency-dependent factor $\chi_k(\nu)$ (see Eq. (A.26)). The above-mentionned set of approximations, after tedious calculations, leads us to (see details in Appendix A)

$$\mathcal{F}_\tau(\tau, \nu) = \left(\frac{\sigma_\tau^2}{\nu_0}\right) S_\Theta(\tau, \nu), \tag{9}$$

where

$$\sigma_\tau = \frac{12}{\sqrt{2}} \sqrt{\frac{\tau_g}{N_g}}\, \Theta^2_{\rm rms}, \quad \tau_g = \kappa \rho \Lambda, \quad N_g = \frac{2\pi R_s^2}{\Lambda^2}, \tag{10}$$

$\Theta_{\rm rms}$ the root-mean-square of Θ (Eq. (A.25)), and Λ a characteristic length (see below). Note that in Eq. (10), τ_g corresponds to the characteristic optical thickness of the granules, N_g to the average number of granules distributed over half of the photosphere (i.e., at $r = R_s$), and σ_τ to the global brightness fluctuations associated with the granulation spectrum that one would see at the optical depth τ. The RHS of Eq. (9) involves the dimensionless source function $S_\Theta(\tau, \nu)$, whose expression is given in Eq. (A.32). The latter depends on $E_\Theta(k)$ and $\chi_k(\nu)$.

The adopted expression for the spatial spectrum $E_\Theta(k)$ (see Eq. (A.38)) involves the length-scale Λ as well as the characteristic wavenumber k_c, which separates the inertial-convective range from the inertial-conductive range. Some prescriptions are required for Λ and k_c, however. We hence assume that $\Lambda = \beta H_p$, where H_p is the pressure scale height and β a free parameter. For k_c, we adopt the prescription $k_c = \zeta \left(\frac{\epsilon}{\chi^3_{\rm rad}}\right)^{1/4}$, where ζ is a free parameter introduced to exert some control on this prescription, $\chi_{\rm rad}$ is the radiative diffusivity coefficient, and ϵ is the rate of injection of kinetic energy into the turbulent cascade.

We turn now to the frequency component $\chi_k(\nu)$. In a strongly turbulent medium, χ_k is well described by a Lorentzian function

$$\chi_k(\nu) = \frac{1}{\pi \nu_k} \frac{1}{1 + (\nu/\nu_k)^2}, \tag{11}$$

where ν_k is by definition the half-width at half-maximum of $\chi_k(\nu)$. The expression for ν_k is given in Eq. (A.45), which involves the free parameter λ. This was introduced to have some control on this definition. As an alternative for a Lorenztian function (see Appendix A.4.2), we also consider an exponential form

$$\chi_k(\nu) = \frac{\ln 2}{2\,\nu_k} \exp\left[-\left|\ln 2 \frac{\nu}{\nu_k}\right|\right]. \tag{12}$$

3. Calibration using solar observations

The theoretical granulation representative of the Sun were computed on the basis of the present model using inputs extracted from a 3D hydrodynamical model of the solar surface layers. To reproduce the solar observations, we calibrated the free parameters involved in the theory.

3.1. Computation details

We computed the theoretical PDS of the granulation ($\mathcal{F}$) according to Eqs. (7), (9), and (10) together with Eq. (A.15) and the set of Eqs. (A.32)–(A.36). The different quantities involved in the theoretical model (stratification, convective velocity, etc.) were obtained from a 3D model in a similar way as in Samadi et al. (2003b). However, while Samadi et al. (2003b) extracted these quantities from horizontal averages at constant geometrical depth, we here performed the averages at a constant optical depth τ. This is justified because the RHS of Eq. (7) is integrated over the optical depth.

For later use, we define σ as the root-mean-square (rms) brightness fluctuations associated with a given PDS. The latter satisfies the following relation

$$\sigma^2 = \int_{-\infty}^{+\infty} {\rm d}\nu\, \mathcal{F}(\nu), \tag{13}$$

where $\mathcal{F}(\nu)$ refers to a given PDS. Another important characteristic of the granulation spectrum is its associated timescale $\tau_{\rm eff}$, which is here defined, following Mathur et al. (2011), as the e-folding time associated with the auto-correlation function (ACF) of the relative flux variations caused by the granulation. Different PDS are next compared, in terms of their shape (i.e., ν variation), σ and $\tau_{\rm eff}$.

We considered a 3D model representative of the surface layers of the Sun (see details in Ludwig et al. 2009) and computed the associated theoretical PDS. This was then compared with the PDS obtained from the green channel of the SOHO/VIRGO three-channel sun-photometer (SPM, see Frohlich et al. 1997). We multiplied the original data by the instrumental function response function as derived by Michel et al. (2009) to convert the observed photometric fluctuations in terms of bolometric ones. To compare theoretical PDS with the observations, we systematically added the instrumental whited noise component, which we measured at high frequency on the observed solar spectrum.

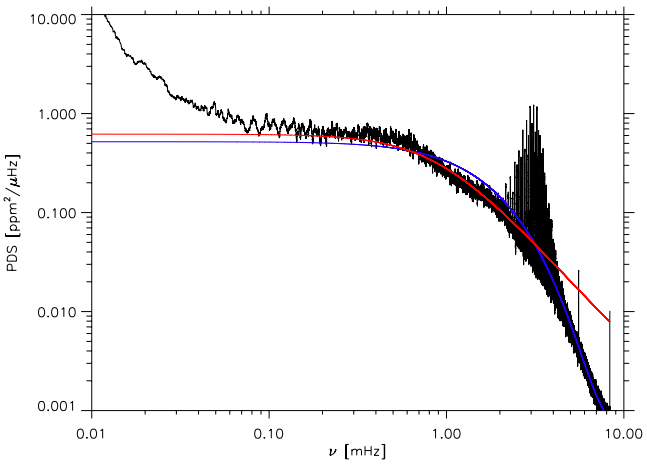

Fig. 1. Power density spectrum in ppm^2/μHz as a function of frequency ν. In black: PDS obtained from the green channel of the SOHO/VIRGO three-channel sun-photometer. In red and blue: theoretical PDS of the granulation background ($\mathcal{F}$) computed using the quantities obtained from the solar 3D model. The red curve assumes a Lorentzian function for χ_k, the blue curve an exponential functional.

3.2. Lorentzian versus exponential χ_k

We first assumed by default $\lambda = 1, \beta = 1$ and $\zeta = 1$ and adopted a Lorentzian shape for χ_k (Eq. (11)). The theoretical PDS underestimates σ by a factor of about 30 and the width of the solar granulation by a factor about five (not shown). Part of this significant discrepancy is due to our prescription for Λ (Eq. (A.42)), k_c (Eq. (A.43)), and ν_k (Eq. (A.45)). The estimation of these quantities can been controlled by the parameters β and ζ, and the product $\beta\lambda$, respectively. However, there is some degeneracy between ζ and β (see below). At fixed value of ζ, we then simultaneously adjusted β and $\beta\lambda$ such that σ and the width of the spectrum best matches the observations. This led to $\beta = 14.8$ and $\lambda\beta = 3.7$. The resulting theoretical PDS is shown in Fig. 1.

We obtained an overall satisfactory agreement between the theoretical PDS and the observations, except for the frequency variations at high frequencies.

There are several pieces of observational evidence that the granulation spectrum significantly departs at high frequencies from a Lorentzian function (e.g., Mathur et al. 2011, and references therein). Furthermore, calculations performed with the Ludwig (2006) method also confirm this general trend (Ludwig et al. 2009; Ludwig & Steffen 2012). Accordingly, we now considered the exponential function given by Eq. (12). The free parameter β and the product $\beta\,\lambda$ were adjusted such that the theoretical PDS reproduces the observations best. For this we fitted the observed solar spectrum by means of the maximum-likelihood estimator (see e.g. Toutain & Appourchaux 1994; Appourchaux et al. 1998). For $\zeta = 1$, the fit leads to $\beta = 7.8$ and $\beta\,\lambda = 3.0$. As seen in Fig. 1, we obtained an overall satisfactory agreement with the observations. In particular, the observations are much better fitted at high frequencies than when a Lorentzian function is adopted. Consequently, unless mentioned otherwise, we adopted the exponential function from now on.

Other values of the parameter ζ were also tested. For each adopted value of ζ, we have adjusted the parameter β and the product $\beta\,\lambda$ such as to reproduce the solar data best. They all result in almost the same agreement with the solar observations. As for the Lorentzian χ_k (see Sect. 3.2), there is thus a degeneracy between the parameters β and ζ. Therefore, the observed solar granulation background does not permit one to constrain these parameters independently. However, the granules observed on the solar surface have a typical size of about 2 Mm (see e.g. Muller 1989; Roudier et al. 1991). Furthermore, the observations reported by Espagnet et al. (1993) and Hirzberger et al. (1997) suggest that $k_c/k_0 \approx 2$. These observations accordingly favor a value of ζ of about five since this value results in $k_c/k_0 = 1.9$ and $\Lambda = 1.7$ Mm. In the following we therefore assumed $\zeta = 5$. The corresponding value of β is 12.3, which value is within the range found by Trampedach et al. (2013), that is, 9–13.

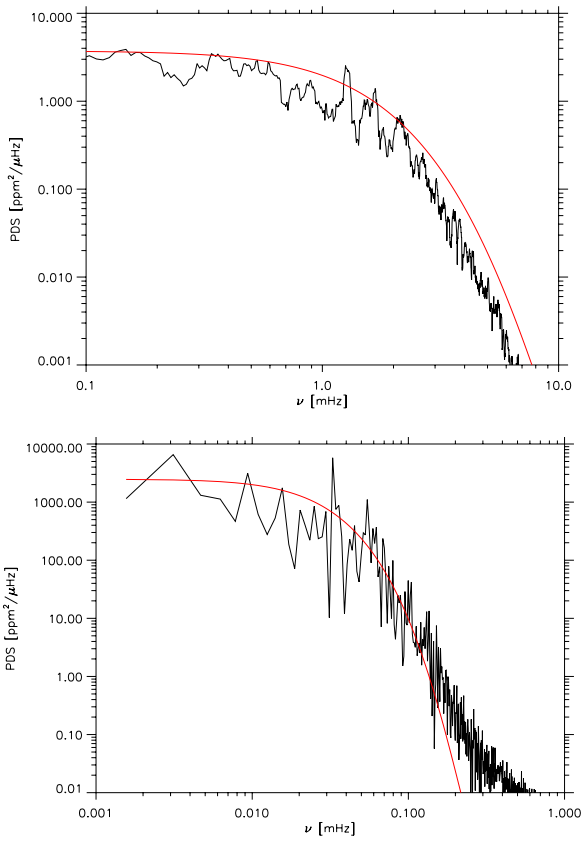

Fig. 2. *Top*: power density spectrum in ppm^2/μHz as a function of frequency ν obtained for a 3D RHD model representative of an F-dwarf star (see Sect. 4.1). The black curve corresponds to the theoretical PDS obtained by Ludwig et al. (2009) on the basis of the ab initio approach, the red curve to the PDS obtained with our theoretical model using inputs extracted from the same 3D model (see Sect. 3.1). *Bottom*: same as the top panel for the 3D model representative of a red-giant star (see Sect. 4.2).

4. Comparison with the Ludwig (2006) ab initio modeling

We compare here theoretical PDS computed with calculations performed on the basis of the Ludwig (2006) ab initio modeling assuming the same 3D hydrodynamical models in both cases. Two different 3D models were considered: a 3D model representative of the surface layers of an F-type main-sequence star (Sect. 4.1) and a second representative of the surface layers of a red giant star (Sect. 4.2). These 3D models constitute two extreme cases in the H-R diagram.

Because calculation of the PDS requires knowing the stellar radius R_s, this was obtained by matching a complete 1D standard model to the stratification of the 3D model (see details in Trampedach 1997; Samadi et al. 2008). The standard 1D model was computed using the CESAM2K code (Morel & Lebreton 2008).

4.1. F-type main-sequence stellar model

Ludwig et al. (2009) have computed two F-dwarf 3D models that included the CoRoT target HD 49933 in terms of surface metal abundance. Of these two 3D models, we considered here the one with the solar surface abundance. This model has $T_{\rm eff} = 6725$ K and $\log g = 4.25$. We computed the theoretical PDS as detailed in Sect. 3.1. We adopted the values of the free parameters that give the best agreement between the model and the observations for the Sun (see Sect. 3). The result of the calculation is presented in Fig. 2 (top panel).

We compared the theoretical PDS with the spectrum obtained by Ludwig et al. (2009) on the basis of the ab initio method. Their calculation was based on a radius of $R_{\rm S,Ludwig} = 1.35\,R_\odot$, while our associated global 1D model has a radius of $R_{\rm S} = 1.473\,R_\odot$. To compare ours with their results, we multiplied their spectrum by $(R_{\rm S,Ludwig}/R_{\rm S})^2$ since the PDS is inversely proportional to the square of the radius (Ludwig 2006). The resulting PDS is shown in Fig. 2 (top panel).

The ν-variation of the PDS obtained with the ab initio approach is well reproduced. For the characteristic time $\tau_{\rm eff}$, our theoretical calculations result in a value of $\tau_{\rm eff}$ 5% lower than for Ludwig et al. (2009). The rms of the global brightness fluctuations associated with their spectrum is $\sigma = 84 \pm 17$ ppm. Our theoretical model results in an rms brightness fluctuation of $\sigma = 97.4$ ppm. This is about 16% higher than the result of Ludwig et al. (2009). It is worth mentioning that, consistently with the Ludwig et al. (2009) results, our model also results in a significant overestimation of the measured σ for this F-dwarf star. Furthermore, we show in Paper II that our theoretical model results for F-dwarf stars in a systematic overestimation of σ. As discussed in Paper II, this trend is very likely linked to the impact of the high level of magnetic activities on the surface convection

(see also Chaplin et al. 2011a,b). We therefore emphasize that all our calculations must be rigorously considered to be valid only for stars with a low activity level.

4.2. Red giant model

We considered a 3D model of the surface layers of a red-giant star characterised by $\log g = 2.5$ and $T_{\rm eff} = 4964 \pm 22$ K (see details in Ludwig & Steffen 2012). The associated theoretical PDS is compared in Fig. 2 (bottom panel) with the PDS computed by Ludwig & Steffen (2012) on the basis on the Ludwig (2006) ab initio approach. Their calculation assumed a radius $R_{\rm S,Ludwig} = 10\,R_\odot$, while our associated global 1D model has a radius of $R_{\rm s} = 17.8\,R_\odot$. Accordingly, we multiplied their PDS by $(R_{\rm S,Ludwig}/R_{\rm s})^2$.

Except at very high frequency ($\nu \gtrsim 150\ \mu$Hz), we obtain a good match between the two calculations, both in terms of amplitude and ν-variation. Our theoretical spectrum results in $\sigma = 352$ ppm, which is only 9% higher than the one obtained by Ludwig & Steffen (2012). For $\tau_{\rm eff}$, we obtain $\tau_{\rm eff} = 1.01 \times 10^4$ s. This is 29% higher than the value derived from the Ludwig & Steffen (2012) PDS.

We note that assuming different sets of the calibrated parameters (see Sect. 3.2) has a negligible impact on the ν-variation of the PDS and a moderate effect on σ, for both the red giant and F-dwarf models. Furthermore, for both 3D models, assuming a Lorenztian function for $\chi_k(\nu)$ instead of an exponential function, results in a considerable discrepancy at high frequency, as in the case of the Sun (not shown).

5. Conclusion

We have developed a simple 1D theoretical model for the granulation spectrum. One advantage of this model is that it can be used to compute theoretical granulation spectra on a large scale. Another benefit is that any prescription for the turbulent spectrum can been considered, in particular, different prescriptions can be tested for χ_k, the Fourier transform of the time correlation function of the eddy velocity at a fixed k wavenumber. In this way, we have established a link between the ν-variation of the granulation spectrum in intensity with the frequency component χ_k.

The theoretical model was first applied to the solar case. The stratification of the surface layers of the Sun and the properties of its surface convection were obtained from a 3D hydrodynamical model of the surface layers of the Sun. Assuming default values for the free parameters involved in the theoretical model, our theoretical model strongly underestimates the quantities σ and $\tau_{\rm eff}$ derived from the observed solar granulation spectrum. Nevertheless, the solar granulation spectrum can be well reproduced by adjusting two of the three free parameters involved in the theoretical model, while the degeneracy between the free parameters was removed by using constraints from solar images.

Two different functions for $\chi_k(\nu)$ were tested: a Lorentzian function and an exponential one. Whatever the choice of the free parameters, the ν-variation of the solar spectrum is not reproduced at high frequencies with the Lorentzian function. Indeed, at high frequencies the theoretical spectrum decreases as ν^{-2}, while the observations decrease much more rapidly with ν. On the other hand, adopting an exponential χ_k results in a much better agreement at high frequency. As discussed in Appendix C, this result confirms the previous claim by Nordlund et al. (1997) that the granules seen in the visible part of the atmosphere have a low level of turbulence.

We then compared theoretical PDS with PDS calculated on the basis of the Ludwig (2006) ab inito approach, that is from the timeseries of the intensity emerging directly from 3D hydrodynamical models of the surface layers of stars. The time-averaged properties of the surface layers were obtained from two 3D hdyrodynamical models, one representative of an F-type star and the second one for a red giant star. The theoretical PDS reproduces the main characteristics of the PDS obtained with the ab initio modeling. As in the solar case, the best agreement was obtained with an exponential $\chi_k(\nu)$.

However, some residual differences remain between our theoretical calculations and the solar granulation spectrum as well as between our calculations and those obtained with the ab initio approach. As discussed in Appendix D, all these differences do not exhibit a severe defect of our theoretical model, however, and we conclude that the main physical assumptions of the theoretical model are validated by our different comparisons. Further theoretical developments are required to improve the modeling of the granulation background, however.

We compute in the companion paper on the basis of this theoretical model the global brightness fluctuations (σ) and the lifetime ($\tau_{\rm eff}$) associated with the stellar granulation for a set of stars with different spectral types and luminosity classes. This will then allow us to derive theoretical scaling laws for σ and $\tau_{\rm eff}$, which we then compare with *Kepler* observations.

Acknowledgements. SOHO is a mission of international collaboration between ESA and NASA. R.S. and K.B. acknowledge financial support from the Programme National de Physique Stellaire (PNPS) of CNRS/INSU and from Agence Nationale de la Recherche (ANR, France) program "Interaction Des Étoiles et des Exoplanètes" (IDEE, ANR-12-BS05-0008). HGL acknowledges financial support by the Sonderforschungsbereich SFB 881 "The Milky Way System" (subproject A4) of the German Research Foundation (DFG). RS thanks Frédéric Baudin for useful discussions about statistical issues.

References

Aigrain, S., Favata, F., & Gilmore, G. 2004, in Stellar Structure and Habitable Planet Finding, eds. F. Favata, S. Aigrain, & A. Wilson, ESA SP, 538, 215
Andersen, B., Leifsen, T., Appourchaux, T., et al. 1998, in Structure and Dynamics of the Interior of the Sun and Sun-like Stars, ed. S. Korzennik, ESA SP, 418, 83
Appourchaux, T., Gizon, L., & Rabello-Soares, M.-C. 1998, A&AS, 132, 107
Appourchaux, T., Belkacem, K., Broomhall, A.-M., et al. 2010, A&ARv, 18, 197
Balmforth, N. J. 1992, MNRAS, 255, 639
Belkacem, K., Samadi, R., Goupil, M. J., & Kupka, F. 2006, A&A, 460, 173
Belkacem, K., Samadi, R., Goupil, M. J., et al. 2010, A&A, 522, L2
Belkacem, K., Goupil, M. J., Dupret, M. A., et al. 2011, A&A, 530, A142
Bray, R. J., & Loughhead, R. E. 1967, The solar granulation
Brown, T. M., Gilliland, R. L., Noyes, R. W., & Ramsey, L. W. 1991, ApJ, 368, 599
Chaplin, W. J., Bedding, T. R., Bonanno, A., et al. 2011a, ApJ, 732, L5
Chaplin, W. J., Kjeldsen, H., Bedding, T. R., et al. 2011b, ApJ, 732, 54
Espagnet, O., Muller, R., Roudier, T., & Mein, N. 1993, A&A, 271, 589
Freytag, B., Holweger, H., Steffen, M., & Ludwig, H.-G. 1997, in Science with the VLT Interferometer, ed. F. Paresce (Berlin, New York: Springer Verlag), 316
Frohlich, C., Andersen, B. N., Appourchaux, T., et al. 1997, Sol. Phys., 170, 1
Georgobiani, D., Stein, R. F., & Nordlund, Å. 2006, in Solar MHD Theory and Observations: A High Spatial Resolution Perspective, eds. J. Leibacher, R. F. Stein, & H. Uitenbroek, ASP Conf. Ser., 354, 109
Gray, D. 1992, The observation and analysis of stellar photospheres (Cambridge University Press)
Harvey, J. W., Duvall, Jr., T. L., Jefferies, S. M., & Pomerantz, M. A. 1993, in GONG 1992. Seismic Investigation of the Sun and Stars, ed. T. M. Brown, ASP Conf. Ser., 42, 111

Hirzberger, J., Vazquez, M., Bonet, J. A., Hanslmeier, A., & Sobotka, M. 1997, ApJ, 480, 406
Huber, D., Stello, D., Bedding, T. R., et al. 2009, Communications in Asteroseismology, 160, 74
Kallinger, T., & Matthews, J. M. 2010, ApJ, 711, L35
Karoff, C. 2012, MNRAS, 421, 3170
Kjeldsen, H., & Bedding, T. R. 1995, A&A, 293, 87
Kjeldsen, H., & Bedding, T. R. 2011, A&A, 529, L8
Kupka, F., & Robinson, F. J. 2007, MNRAS, 374, 305
Lesieur, M. 1997, Turbulence in fluids (Kluwer Academic Publishers)
Ludwig, H. 2006, A&A, 445, 661
Ludwig, H.-G., & Steffen, M. 2012, 3D Model Atmospheres of Red Giant Stars, eds. A. Miglio, J. Montalbán, & A. Noels (Berlin, Heidelberg: Springer Verlag), 125
Ludwig, H., Samadi, R., Steffen, M., et al. 2009, A&A, 506, 167
Mathur, S., Hekker, S., Trampedach, R., et al. 2011, ApJ, 741, 119
Matthews, J. M., Kuschnig, R., Guenther, D. B., et al. 2004, Nature, 430, 51
Michel, E., Baglin, A., Auvergne, M., et al. 2008, Science, 322, 558
Michel, E., Samadi, R., Baudin, F., et al. 2009, A&A, 495, 979
Millionshchikov, M. D. 1941, Doklady Acad. Nauk SSSR, 32, 611
Monin, A. S., & Yaglom, A. M. 1971, Statistical Fluid mechanics: Mechanics of turbulence, ed. J. L. Lumley (Dover publications), 2
Morel, P., & Lebreton, Y. 2008, Ap&SS, 316, 61
Mosser, B., Belkacem, K., Goupil, M.-J., et al. 2010, A&A, 517, A22
Muller, R. 1989, in Solar and Stellar Granulation, eds. R. Rutten, & G. Severino (Kluwer Academic Publishers), 101
Muller, R. 1999, in Motions in the Solar Atmosphere, eds. A. Hanslmeier, & M. Messerotti, Astrophys. Space Sc. Lib., 239, 35
Musielak, Z. E., Rosner, R., Stein, R. F., & Ulmschneider, P. 1994, ApJ, 423, 474
Nordlund, A., Spruit, H. C., Ludwig, H.-G., & Trampedach, R. 1997, A&A, 328, 229
Nordlund, Å., Stein, R. F., & Asplund, M. 2009, Liv. Rev. Sol. Phys., 6, 2
Ogura, Y. 1963, J. Fluid Mech., 16, 33
Roudier, T., Vigneau, J., Espagnet, O., et al. 1991, A&A, 248, 245
Samadi, R. 2011, in Lect. Notes Phys., 832, The Pulsations of the Sun and the Stars, eds. J.-P. Rozelot, & C. Neiner (Berlin Springer Verlag)
Samadi, R., & Goupil, M. J. 2001, A&A, 370, 136
Samadi, R., Nordlund, Å., Stein, R. F., Goupil, M. J., & Roxburgh, I. 2003a, A&A, 404, 1129
Samadi, R., Nordlund, Å., Stein, R. F., Goupil, M. J., & Roxburgh, I. 2003b, A&A, 403, 303
Samadi, R., Belkacem, K., Goupil, M. J., Dupret, M.-A., & Kupka, F. 2008, A&A, 489, 291
Samadi, R., Belkacem, K., Ludwig, H.-G., et al. 2013, A&A, 559, A40
Sawford, B. L. 1991, Phys. Fluids, 3, 1577
Siedentopf, H. 1933, Astron. Nachr., 247, 297
Stein, R. F. 1967, Sol. Phys., 2, 385
Stello, D., Chaplin, W. J., Basu, S., Elsworth, Y., & Bedding, T. R. 2009, MNRAS, 400, L80
Svensson, F., & Ludwig, H.-G. 2005, in 13th Cambridge Workshop on Cool Stars, Stellar Systems and the Sun, eds. F. Favata, G. A. J. Hussain, & B. Battrick, ESA SP, 560, 979
Toutain, T., & Appourchaux, T. 1994, A&A, 289, 649
Trampedach, R. 1997, Master's thesis, Master's thesis, Aarhus University
Trampedach, R., Asplund, M., Collet, R., Nordlund, Å., & Stein, R. F. 2013, ApJ, 769, 18
Unsöld, A. 1930, ZAp, 1, 138
Vázquez Ramió, H., Régulo, C., & Roca Cortés, T. 2005, A&A, 443, L11

Pages 7 to 10 are available in the electronic edition of the journal at http://www.aanda.org

Appendix A: Theoretical developments

A.1. General expression of the PDS

We establish here our general expression of the PDS, that it is Eqs. (7) and (8). We start from the term of Eq. (6), which enters in the RHS of Eq. (1). We apply the operator given by Eq. (2) on Eq. (6), it gives

$$\widehat{\Delta F}(\nu) \;=\; R_{\rm s}^2 \int \frac{{\rm d}^3\boldsymbol{r}}{r^2} \int_{-T_0/2}^{T_0/2} {\rm d}t\; \rho\kappa\, {\rm e}^{-\tau(r)/\mu}\, {\rm e}^{{\rm i}\,2\pi\nu t}\, \Delta B(t,\boldsymbol{r}), \quad \text{(A.1)}$$

where the space integration is performed over half of the (stellar) sphere, ${\rm d}^3r = -{\rm d}\mu\, r^2\, {\rm d}r\, {\rm d}\phi$, and ${\rm d}\tau = \kappa\,\rho$.

The extent of the region where the stellar granulation is seen is very small compared to the stellar radius $R_{\rm s}$, such that r is almost constant over the optical depth range relevant for calculating the flux. Therefore, in very good approximation we have $(R_{\rm s}/r)^2 \simeq 1$ in the integrand of Eq. (A.1). Accordingly, Eq. (A.1) can be simplified as

$$\widehat{\Delta F}(\nu) \;=\; \int {\rm d}^3\boldsymbol{r} \int_{-T_0/2}^{T_0/2} {\rm d}t\; \rho\kappa\, {\rm e}^{-\tau(r)/\mu}\, {\rm e}^{{\rm i}\,2\pi\nu t}\, \Delta B(t,\boldsymbol{r}). \quad \text{(A.2)}$$

Since $\widehat{\Delta F}(\nu)$ cannot be evaluated in a deterministic way but a statistical one only, we consider the square of Eq. (A.2) and average it over a large number of independent realizations. This gives

$$\begin{aligned}\langle|\widehat{\Delta F}|^2\rangle(\nu) \;=\; & \int {\rm d}^3\boldsymbol{r}_1\, \kappa(r_1)\rho(r_1)\, {\rm e}^{-\tau(r_1)/\mu(\boldsymbol{r}_1)} \int_{t_1=-T_0/2}^{T_0/2} {\rm d}t_1\, {\rm e}^{{\rm i}\,2\pi\nu t_1} \\ & \times \int {\rm d}^3\boldsymbol{r}_2\, \kappa(r_2)\rho(r_2)\, {\rm e}^{-\tau(r_2)/\mu(\boldsymbol{r}_2)} \int_{t_2=-T_0/2}^{T_0/2} {\rm d}t_2\, {\rm e}^{-{\rm i}\,2\pi\nu t_2} \\ & \times \langle \Delta B_1\, \Delta B_2\rangle, \end{aligned} \quad \text{(A.3)}$$

where ΔB_1 (resp. ΔB_2) corresponds to the quantity ΔB evaluated at the time-space position $(t_1, \boldsymbol{r}_1)$ (resp. $(t_2, \boldsymbol{r}_2)$).

We then define the following new coordinates

$$t_0 = (t_1 + t_2)/2 \qquad t' = t_2 - t_1, \quad \text{(A.4)}$$

$$\boldsymbol{r}_0 = (\boldsymbol{r}_1 + \boldsymbol{r}_2)/2 \qquad \boldsymbol{r} = \boldsymbol{r}_2 - \boldsymbol{r}_1. \quad \text{(A.5)}$$

In these coordinates, $\boldsymbol{r}$ and t' are the spatial correlation and temporal correlation lengths associated with the local properties of the turbulence, while $\boldsymbol{r}_0$ and t_0 are mean space and time positions. Using the new coordinates given by Eqs. (A.4) and (A.5) in Eq. (A.6) leads to

$$\begin{aligned}\langle|\widehat{\Delta F}|^2\rangle(\nu) = 2\pi \int \int_{-T_0/2}^{T_0/2} {\rm d}t_0\, {\rm d}^3\boldsymbol{r}_0 \\ \times\; \kappa(r_0)\,\rho(r_0)\, {\rm e}^{-2\tau_0/\mu_0}\, \Gamma(t_0, \boldsymbol{r}_0, \nu),\end{aligned} \quad \text{(A.6)}$$

where

$$\Gamma(t_0, \boldsymbol{r}_0, \nu) = \int {\rm d}^3\boldsymbol{r}\, \frac{\gamma(\boldsymbol{r}_0, \boldsymbol{r})}{2\pi} \int_{T_0/2}^{T_0/2} {\rm d}t'\, {\rm e}^{-{\rm i}\,2\pi\nu t'}\, \langle \Delta B_1\, \Delta B_2\rangle \quad \text{(A.7)}$$

$$\gamma(\boldsymbol{r}_0, \boldsymbol{r}) = \frac{\kappa(r_1)\rho(r_1)\,\kappa(r_2)\,\rho(r_2)}{\kappa(r_0)\rho(r_0)}\, {\rm e}^{2\tau_0/\mu_0 - (\tau_1/\mu_1 + \tau_2/\mu_2)} \quad \text{(A.8)}$$

and $\tau_i = \tau(r_i)$, $\mu_i = \mu(\boldsymbol{r}_i)$ with $i = \{0, 1, 2\}$.

At this stage, a tractable expression for Eq. (A.6) calls for more assumptions. We assume that T_0 is much longer than the granule lifetime. We neglect length-scales longer than the granulation length-scales. In that case ΔB represents the instantaneous difference between the brightness of the granules situated at the position $(\tau(r), \mu, \phi)$ and the brightness of the material in the steady state ($< B >_t$). Accordingly, Eq. (A.6) reduces to

$$\langle|\widehat{\Delta F}|^2\rangle = (2\pi)^2\; R_{\rm s}^2\; T_0 \int_0^1 {\rm d}\mu_0 \int_0^{+\infty} {\rm d}\tau_0\, {\rm e}^{-2\tau_0/\mu_0}\, \Gamma(\tau_0, \nu) \quad \text{(A.9)}$$

$$\Gamma(\tau_0, \nu) = \int {\rm d}^3\boldsymbol{r}\, \frac{\gamma(r_0, r)}{2\pi} \int_{-\infty}^{+\infty} {\rm e}^{-{\rm i}\,2\pi\nu t'}\, \langle \Delta B_1\, \Delta B_2\rangle\, {\rm d}t' \quad \text{(A.10)}$$

$$\gamma(r_0, r) = \frac{\kappa(r_1)\rho(r_1)\,\kappa(r_2)\rho(r_2)}{\kappa(r_0)\rho(r_0)}. \quad \text{(A.11)}$$

We now assume that $\kappa\rho$ varies at a length-scale longer than the characteristic size of the granules. This assumption is discussed in Appendix B. Accordingly, $\gamma \simeq \kappa(r_0)\rho(r_0)$ and Γ reduces to

$$\Gamma(\tau_0, \nu) = (2\pi)^2\, \kappa(\tau_0)\rho(\tau_0)\, \langle \widetilde{\Delta B_1\, \Delta B_2}\rangle(\nu, \boldsymbol{k} = \boldsymbol{0}), \quad \text{(A.12)}$$

where $\langle \widetilde{\Delta B_1\, \Delta B_2}\rangle$ is the space and time Fourier transform of $\langle \Delta B_1\, \Delta B_2\rangle$, defined as

$$\langle \widetilde{\Delta B_1\, \Delta B_2}\rangle(\nu, \boldsymbol{k}) \equiv \frac{1}{(2\pi)^3} \int {\rm d}t' \int {\rm d}^3 r\, {\rm e}^{-2{\rm i}\pi\nu t' - {\rm i}\boldsymbol{k}.\boldsymbol{r}}\, \langle \Delta B_1\, \Delta B_2\rangle. \quad \text{(A.13)}$$

Note that, from now on, we substitute the notation τ_0 by τ.

We now turn to the time-averaged flux $\langle F\rangle_t$. From Eqs. (3), (4), and (5) one derives

$$\langle F\rangle_t = 2\pi\, R_{\rm s}^2\, F_0, \quad \text{(A.14)}$$

where we have defined

$$F_0 \equiv \int_0^1 {\rm d}\mu \int_0^{+\infty} {\rm d}\tau\, {\rm e}^{-\tau/\mu}\, \langle B\rangle_t(\tau). \quad \text{(A.15)}$$

Finally, using Eq. (A.9), Eq. (A.12) and Eq. (A.14) we derive the general expressions of Eqs. (7) and (8). The term $\mathcal{F}_\tau$ (Eq. (8)) stands for the PDS of the granulation as it would be seen at the optical depth τ. However, the *observed* PDS associated with the granulation background is given by Eq. (7) and corresponds to the sum of the spectra seen at different layers in the atmosphere, but weighted by the term ${\rm e}^{-2\tau/\mu}\ (\langle B\rangle_t/F_0)^2$.

A.2. Source function ($\langle \Delta B_1\, \Delta B_2\rangle$)

To proceed we need to derive an expression for the correlation product $\langle \Delta B_1\, \Delta B_2\rangle$. To this end, we recall that $B = \sigma T^4/\pi$, where σ is the Stefan-Boltzmann constant, and introduce ΔT as the difference between the temperature of the granule and that of the surrounding medium. We thus have

$$\Delta B = \left((1+\Theta)^4 - 1\right) \langle B\rangle_t\,, \quad \text{(A.16)}$$

where $\Theta \equiv \Delta T/\langle T\rangle_t$. The second-order Taylor expansion of the RHS of Eq. (A.16) gives

$$\Delta B = \left(4\,\Theta + 6\,\Theta^2\right) \langle B\rangle_t. \quad \text{(A.17)}$$

We have neglected the third and fourth order terms in Θ. Indeed, a 3D hydrodynamical simulation of the solar surface shows that terms higher than second order contribute less than about 15% of Eq. (A.16). Accordingly,

$$\begin{aligned}\langle \Delta B_1\, \Delta B_2\rangle \;=\; & 4\left(4\,\langle \Theta_1\, \Theta_2\rangle + 9\langle \Theta_1^2\, \Theta_2^2\rangle + 6\langle \Theta_1\, \Theta_2^2\rangle \right. \\ & \left. + 6\langle \Theta_2\, \Theta_1^2\rangle\right) \langle B\rangle_t^2, \end{aligned} \quad \text{(A.18)}$$

where $\Theta_1 \equiv \Theta(\boldsymbol{r}_1, t_1)$ and $\Theta_2 \equiv \Theta(\boldsymbol{r}_2, t_2)$.

We now adopt the quasi-normal approximation (QNA). This approximation is rigorously valid for normally distributed quantities. Departure from this approximation is discussed in Appendix B. Normally distributed quantities are necessarily symmetric, such that $\langle \Theta_1\, \Theta_2^2 \rangle = 0$ and $\langle \Theta_2\, \Theta_1^2 \rangle = 0$. This approximation also implies (e.g., Lesieur 1997, Chap. VII-2)

$$\langle \Theta_1^2\, \Theta_2^2 \rangle = \langle \Theta_1^2 \rangle \langle \Theta_2^2 \rangle + 2\langle \Theta_1 \Theta_2 \rangle^2. \tag{A.19}$$

The first term in the RHS of Eq. (A.19) does not contribute in the time Fourier domain, except at the null frequency. Accordingly,

$$\langle \Delta B_1\, \Delta B_2 \rangle = \left[16\, \langle \Theta_1 \Theta_2 \rangle + 72 \langle \Theta_1 \Theta_2 \rangle^2\right] \langle B \rangle_t^2. \tag{A.20}$$

Now using the Parseval-Plancherel relation, Eq. (A.20) becomes

$$\langle \Delta\widetilde{B_1}\, \Delta\widetilde{B_2} \rangle(\nu, \boldsymbol{k}) = \langle B \rangle_t^2 \left[16 \langle \widetilde{\Theta_1 \Theta_2} \rangle(\nu, \boldsymbol{k}) + 72\, \widetilde{\mathcal{B}}_\Theta(\nu, \boldsymbol{k})\right], \tag{A.21}$$

with

$$\tilde{\mathcal{B}}_\Theta(\nu, \boldsymbol{k}) \equiv \int \mathrm{d}\nu' \int \mathrm{d}^3 k' \langle \widetilde{\Theta_1 \Theta_2} \rangle(\nu', \boldsymbol{k}') \langle \widetilde{\Theta_1 \Theta_2} \rangle(\nu'', \boldsymbol{k}''), \tag{A.22}$$

where $\nu'' = \nu + \nu'$ and $\boldsymbol{k}'' = \boldsymbol{k} + \boldsymbol{k}'$.

We assume that the scalar Θ is isotropic. Accordingly, the spatial Fourier transform of $\langle \Theta_1 \Theta_2 \rangle(r, \nu)$ is given by (see e.g. Lesieur 1997, Chap. V-10)

$$\langle \widetilde{\Theta_1 \Theta_2} \rangle(\boldsymbol{k}, \nu) = \frac{E_\Theta(k, \nu)}{2\pi k^2}. \tag{A.23}$$

The scalar spectrum $E_\Theta(k, \omega)$ is related to the scalar variance as (Lesieur 1997, Chap. V-10)

$$\frac{1}{2}\langle \Theta^2 \rangle(\tau) = \frac{1}{2}\Theta_{\rm rms}^2 = \int_{-\infty}^{\infty} \mathrm{d}\nu \int_0^{\infty} \mathrm{d}k\; E_\Theta(k, \nu), \tag{A.24}$$

where $\Theta_{\rm rms}$ is by definition the rms of Θ, which is related to $\Delta T_{\rm rms}$ (the rms of ΔT) according to

$$\Theta_{\rm rms}^2 = \frac{\Delta T_{\rm rms}^2}{\langle T \rangle_t^2}. \tag{A.25}$$

Following Stein (1967), the scalar energy spectrum $E_\Theta(k, \nu)$ can be factorized into a spatial spectrum $E_\Theta(k)$ and a frequency-dependent factor $\chi_k(\nu)$ according to

$$E_\Theta(k, \nu) = E_\Theta(k)\, \chi_k(\nu), \tag{A.26}$$

where the frequency-dependent factor $\chi_k(\nu)$ is normalized such that

$$\int_{-\infty}^{+\infty} \mathrm{d}\nu\, \chi_k(\nu) = 1. \tag{A.27}$$

A.3. Final expression of relative flux variations

The final expression for the term $\mathcal{F}_\tau$ (Eq. (8)) that appears in the RHS of Eq. (7) is obtained by inserting Eq. (A.21) to (A.23) into Eq. (8), so that

$$\mathcal{F}_\tau(\tau, \nu) = \frac{(2\pi)^2\, \kappa\rho}{R_{\rm s}^2} \left[16\, \langle \widetilde{\Theta_1 \Theta_2} \rangle + 72\, \tilde{\mathcal{B}}_\Theta\right], \tag{A.28}$$

where the two terms in the RHS of Eq. (A.28) are considered for $(\tau, \nu, k = 0)$.

Equation (A.28) can be further simplified by assuming that the temperature fluctuations behave as a passive scalar (see Appendix A.4.1 and the discussion in Appendix B). In that case, it can been shown that the first term in the RHS of Eq. (A.28) vanishes (see Monin & Yaglom 1971, Chap. 14.5). Accordingly, Eq. (A.28) simplifies as

$$\mathcal{F}_\tau(\tau, \nu) = \frac{72\, (2\pi)^2\, \kappa\rho}{R_{\rm s}^2}\, \tilde{\mathcal{B}}_\Theta(\tau, \nu, k = 0), \tag{A.29}$$

with

$$\tilde{\mathcal{B}}_\Theta(\tau, \nu, 0) = \frac{1}{\pi} \int \mathrm{d}k \left(\frac{E_\Theta(k)}{k}\right)^2 \psi_k(\tau, \nu)\,, \tag{A.30}$$

$$\psi_k(\tau, \nu) = \int \mathrm{d}\nu'\, \chi_k(\nu')\, \chi_k(\nu' + \nu). \tag{A.31}$$

The final expression, Eq. (A.29), is recast to a more suitable form. To this end, we define the characteristic wave-number $k_0 = 2\pi/\Lambda$ where Λ is a characteristic length. We also define the characteristic frequency $\nu_0 = 1/(2\pi\, \tau_{\rm c})$ where $\tau_{\rm c}$ is a characteristic time. Eventually, Eq. (A.29) leads to Eqs. (9), (10) where we have defined the dimensionless source function

$$S_\Theta(\tau, \nu) = \frac{1}{\pi} \int \frac{\mathrm{d}K}{K^2}\, \tilde{E}_\Theta^2(K)\, \Psi_K(\tau, \xi), \tag{A.32}$$

as well as the following dimensionless quantities:

$$\Psi_K(\tau, \xi) = \int \mathrm{d}\xi'\, \tilde{\chi}_K(\xi')\, \tilde{\chi}_K(\xi' + \xi), \tag{A.33}$$

$$\tilde{E}_\Theta(K) = k_0\, \Theta_{\rm rms}^{-2}\, E_\Theta(k), \tag{A.34}$$

$$\tilde{\chi}_K(\xi) = \nu_0\, \chi_k(\nu), \tag{A.35}$$

$$K = \frac{k}{k_0}, \quad \xi = \frac{\nu}{\nu_0}, \tag{A.36}$$

where we have defined the characteristic wavenumber $k_0 = 2\pi\,/\Lambda$, and the characteristic frequency $\nu_0 = 1/(2\pi\, \tau_{\rm c})$, where $\tau_{\rm c} \equiv 1/(k_0\, u_0)$ is a characteristic time and u_0 a characteristic velocity (see Eq. (A.40) below). Note that the dimensionless quantities $\tilde{E}(K)$ and $\tilde{\chi}_K(\xi)$ verify the following normalization conditions:

$$\int_0^{+\infty} \mathrm{d}K\, \tilde{E}_\Theta(K) = \frac{1}{2}, \quad \text{and} \quad \int_{-\infty}^{+\infty} \mathrm{d}\xi\, \tilde{\chi}_K(\xi) = 1. \tag{A.37}$$

A.4. Turbulence modeling

A.4.1. Spatial spectrum

As already mentioned, it is assumed that the temperature fluctuations behave as a passive scalar (see the discussion in Appendix B). Therefore $E_\Theta(k)$ is given according to (see Lesieur 1997, Chap. VI-10)

$$E_\Theta(k) = \begin{cases} \dfrac{a_0 \Theta_{\rm rms}^2}{u_0^2}\, E(k), & \text{for } k \le k_{\rm c} \\ \dfrac{a_0 \Theta_{\rm rms}^2}{u_0^2} \left(\dfrac{k_{\rm c}}{k}\right)^4 E(k), & \text{for } k > k_{\rm c}, \end{cases} \tag{A.38}$$

where a_0 is a normalization factor, $E(k)$ the kinetic energy spectrum, u_0 a characteristic velocity (see Eq. (A.40) below), and $k_{\rm c}$ the wavenumber, which separates two characteristic ranges:

– the inertial-convective range ($k < k_{\rm c}$). In this domain, advection of the temperature fluctuations by the turbulent velocity field dominates over the diffusion.

– the inertial-conductive range ($k > k_c$). In this domain, the diffusion of the temperature fluctuations dominates over advection.

We consider for $E(k)$ the Kolmogorov spectrum, and the characteristic velocity u_0 is defined such that

$$E(k) = \begin{cases} 0 & \text{for } k < 0 \\ \dfrac{u_0^2}{k_0}\, K^{-5/3} & \text{for } k \geq k_0, \end{cases} \tag{A.39}$$

where the characteristic velocity u_0 is defined such that

$$\frac{3}{2}\, u_0^2 \equiv \int_0^{+\infty} \mathrm{d}k\, E(k). \tag{A.40}$$

From Eq. (A.38) and Eq. (A.39), the spacial spectrum finally becomes

$$\tilde{E}_\Theta(K) = \begin{cases} 0 & \text{for } K < 1 \\ a_0\, K^{-5/3} & \text{for } 1 \leq K \leq K_C \\ a_0\, K_C^4\, K^{-17/3} & \text{for } K_C < K, \end{cases} \tag{A.41}$$

where we have defined $K_C = k_c/k_0$.

Some prescriptions are required for k_c and k_0. 3D RHD show that from one stellar 3D model to another, the granule size Λ scales approximately as the pressure scale-height (H_p) at the photosphere (Freytag et al. 1997). Accordingly, we assume that

$$k_0 = \frac{2\pi}{\Lambda} \quad \text{with} \quad \Lambda = \beta\, H_p, \tag{A.42}$$

where Λ is a characteristic length-scale, H_p the pressure scale height and β is a free parameter. Concerning the characteristic wavenumber k_c, in a medium with very low Prandtl number (which is the case in the stellar medium), k_c is given by (see Lesieur 1997, Chap. VI)

$$k_c = \zeta \left(\frac{\epsilon}{\chi_{\rm rad}^3} \right)^{1/4}, \tag{A.43}$$

where ζ is a free parameters introduced to exercise some control on this prescription, $\chi_{\rm rad}$ is the radiative diffusivity coefficient, and ϵ is the rate of injection of kinetic energy into the turbulent cascade. The latter is estimated according to $\epsilon = \frac{1}{2}\,\Phi\, w^3/\Lambda$, where we have introduced the anisotropy factor $\Phi \equiv \left(u_{\rm rms}^2 + v_{\rm rms}^2 + w_{\rm rms}^2\right)/w_{\rm rms}^2$, where $u_{\rm rms}$, $v_{\rm rms}$, and $w_{\rm rms}$ are the rms of the three components of the velocity (horizontal and vertical ones).

A.4.2. Frequency spectrum

Since in the inertial-convective range (i.e., $k < k_c$) temperature fluctuations are dominated by advection, we assume that – at this scale range – $\chi_k(\nu)$ is the same as the frequency spectrum associated with the velocity field, χ_k^v. This hypothesis tends to be supported by large eddies simulations (see e.g. Samadi et al. 2003a). Indeed, using a solar hydrodynamic simulation, Samadi et al. (2003a) have found that this property is rather well verified by the entropy fluctuations. Since entropy fluctuations are mostly dominated by temperature fluctuations, this must be the same for the temperature fluctuations. For the inertial-conductive range ($k > k_c$): temperature fluctuations are no longer dominated by advection. However, to our knowledge, no study has been conducted yet about the properties of χ_k in this range. Therefore, we assume by default that in this range χ_k varies with ν, as do χ_k^v.

In a strongly turbulent medium, χ_k^v is well described by a Lorentzian function (Sawford 1991; Samadi et al. 2003a; Belkacem et al. 2010), i.e.,

$$\chi_k(\nu) = \frac{1}{\pi \nu_k}\, \frac{1}{1 + (\nu/\nu_k)^2}, \tag{A.44}$$

where ν_k is by definition the half-width at half-maximum of $\chi_k(\nu)$. In the framework of the Samadi & Goupil (2001) formalism, this latter quantity is evaluated as

$$\nu_k = \frac{k\, u_k}{2\pi\lambda}, \tag{A.45}$$

with

$$u_k^2 = \int_k^{2k} E(k)\, \mathrm{d}k, \tag{A.46}$$

where λ is a free parameter introduced, following Balmforth (1992), to have some control on the adopted definition for ν_k. We define the characteristic time $\tau_c \equiv 1/(k_0\, u_0)$, which corresponds to an estimate of the lifetime of the largest eddies. Accordingly, we have $\nu_0 = (2\pi\tau_c)^{-1}$.

The Lorentzian χ_k (Eq. (A.44)) has a justification for a strongly turbulent medium. However, Georgobiani et al. (2006) have found on the basis of a 3D RHD solar model that χ_k decreases more rapidly with ν near the photosphere than it does in deeper layers. Accordingly, as an alternative for a Lorenztian function and following Musielak et al. (1994), we also consider for χ_k an exponential form

$$\chi_k(\nu) = \frac{\ln 2}{2\,\nu_k}\, \exp\left[- \left| \ln 2\, \frac{\nu}{\nu_k} \right| \right], \tag{A.47}$$

where ν_k is the half-width at half-maximum. We alternatively adopted here the two different prescriptions for χ_k.

Appendix B: Approximations and assumptions

Our theoretical model is based on three major approximations and assumptions. They are discussed below.

Passive scalar assumption: it was assumed that the temperature fluctuations behave as a passive scalar. We recall that a passive scalar is a quantity that obeys an equation of diffusion (e.g., Lesieur 1997). For the temperature fluctuations, this equation of diffusion is rigorously valid when the diffusion and the Boussinesq approximations are verified and the stratification is negligible compared with the eddy size. However, all these conditions are not fulfilled in the vicinity of the photosphere where the granules are the more visible. Indeed, in this region the medium is optically thin such that the diffusion approximation does no longer hold. Furthermore, this region is characterized by a non-negligible turbulent Mach number that prevents the Boussinesq approximation from being valid. Finally, the granule sizes are typically of the order of the pressure-scale height (see below). Nevertheless, as shown by Espagnet et al. (1993) and Hirzberger et al. (1997), the spectrum, E_Θ, associated with the temperature fluctuations at the surface of the Sun scales with k as predicted by Eq. (A.38), which was derived assuming that the temperature fluctuations behave as a passive scalar. This suggests that somehow the temperature fluctuations obey an equation of diffusion.

Quasi-normal approximation (QNA): the approximation of Eq. (A.19) assumes that fluctuating quantities are distributed according to a normal distribution. However, it is well known that

the departure from the QNA is important in a strongly turbulent medium (Ogura 1963). Furthermore, the upper-most part of the convection zone is a turbulent convective medium composed of essentially two flows (the granules and the downdraft plumes) that are asymmetric with respect to each other. Therefore, we obviously do not deal with symmetric distribution, as it is the case for a normal distribution. With the help of a solar 3D hydrodynamical simulation, Belkacem et al. (2006) have quantified the departure from the QNA (seee also Kupka & Robinson 2007). However, by comparing 3D hydrodynamical models representative of different main-sequence stars, we have found that this departure does not vary significantly across the main sequence.

Length-scale separation: the derivation of Eq. (7) is based on the assumption that the product $\kappa\rho$ varies at a length-scale significantly longer than the granule size. However, in the case of the Sun, for instance, the granules have a size of about 2 Mm (see e.g. Muller 1989; Roudier et al. 1991) while the pressure-scale height, $H_{\rm p}$, is of the order of few hundred kilometers at the photosphere. Because near the photosphere the density scale-height H_ρ is of the same order as $H_{\rm p}$ and even lower, our assumption does not hold near the photosphere. Nevertheless, 3D hydrodynamic models show that from a stellar model to another, the granule size scales as the pressure scale-height at the photosphere (Freytag et al. 1997; Samadi et al. 2008). Therefore, as for the QNA, we expect that the departure from our hypothesis introduces a bias that remains almost constant across the Hertzsprung-Russell diagram.

The major approximations and assumptions adopted in our model are expected to be in default near the photosphere. However, avoiding these approximations and assumptions would require additional theoretical improvements, and they constitute – at the present time – the only way for deriving an analytical model of the granulation spectrum. We also recall that our objective is to derive a simple analytical model for the interpretation of the observed scaling relations. Furthermore, provided that the three free parameters involved in the model are appropriately tuned, the theoretical model agrees reasonably well with the Ludwig (2006) 3D hydrodynamical approach (see Sect. 4).

Appendix C: Eddy-time correlation

Two different functions for $\chi_k(\nu)$ were tested: a Lorentzian function and an exponential one. For a strongly turbulent medium, one expects a Lorentzian function (Sawford 1991; Samadi et al. 2003a; Belkacem et al. 2010). However, with this function, the theoretical granulation spectrum decreases as ν^{-2}, while the observations decreases much more rapidly with ν. On the other hand, adopting an exponential χ_k results in a much better agreement at high frequency. This is because an exponential χ_k decreases more rapidly with frequency than does a Lorenztian χ_k. Finally, as in the Sun, adopting an exponential χ_k results in a much better match with the theoretical PDS computed with the ab initio approach for two 3D hdyrodynamical models, one representative for an F-type star and the other one for a red giant star (see Sect. 4).

According to Sawford (1991, see also Appourchaux et al. 2010), the time-Fourier transform of the *Lagrangian* eddy-time correlation function is expected to tend to a Lorentzian function when the Reynolds number tends to infinity. In contrast, the less turbulent the medium (i.e., in general the lower Reynolds number), the more rapid the decrease of χ_k with increasing ν. This behavior is also supported for the *Eulerian* eddy-time correlation (χ_k) by hydrodynamical numerical models (see e.g. Samadi 2011). In other words, the ν variation of χ_k is expected to depend on the degree of turbulence. Accordingly, our result confirms that the granules, which are mainly visible near the photosphere, are less turbulent than the super-adiabatic layers situated a few hundred kilometers below the photosphere. We therefore confirm the previous claim by Nordlund et al. (1997) that the granules have a low level of turbulence. This is also consistent with the results by Georgobiani et al. (2006, see also Nordlund et al. 2009). Indeed, these authors showed that χ_k decreases more rapidly with ν near the surface of a solar 3D model than it does in deeper layers, where χ_k is close to a Lorentzian function (Samadi et al. 2003a).

Finally, the fact that the granules have a relatively low level of turbulence is probably not specific to the Sun. Indeed, the 3D RHD models of stars show that the granules have similar properties as in the Sun (e.g., Trampedach et al. 2013). Therefore, it is not surprising that the theoretical PDS computed with the ab initio approach varies with ν in a similar way as in the Sun.

Appendix D: Remaining discrepancies

Although globally satisfactory, the theoretical model does not reproduce the solar granulation spectrum perfectly. Indeed, the observed spectrum shows a kink at $\nu \sim 1$ mHz (see Sect. 3.2). There is no consensus yet about the physical origins of this feature. Depending on the authors, it is either attributed to the occurrence of bright points (e.g., Harvey et al. 1993; Aigrain et al. 2004), the changing properties of the granules (Andersen et al. 1998), a second granulation population (Vázquez Ramió et al. 2005), and finally to faculae (Karoff 2012). A similar discrepancy was obtained by Ludwig et al. (2009) on the basis of the ab initio approach. This indicates that pure hydrodynamical approaches cannot fully account for the observed solar granulation spectrum. Nevertheless, the remaining discrepancies represent only a small fraction of the total brightness fluctuations produced by the granulation phenomenon.

The theoretical model does not perfectly reproduced the PDS obtained with the ab initio approach for the two 3D models considered in this work. For instance, a difference of less than about 15% is obtained for σ with the 3D model for an F-dwarf star and a difference less than about 30% are obtained for $\tau_{\rm eff}$ with the 3D model for a red giant star. These differences must be attributed to the different approximations and assumptions adopted (see Appendix B above). Nevertheless, they remain of the order of the dispersion obtained between the different methods of analysis investigated by Mathur et al. (2011, see also Paper II). Because the ab initio modeling is based on a very limited set of physical hypothesis, the reasonable agreement between the two approaches shows that despite the numerous hypotheses and assumptions adopted in our theoretical model (see Appendix B), our model provides realistic results.